Journal of Molecular Modeling (2022) 28:366
https://doi.org/10.1007/s00894-022-05358-7

ORIGINAL PAPER

Mechanical, electronic, thermodynamic and vibrational properties of X_2MgAl (X = Sc, Ti and Y) from first principles calculations

Nihat Arikan[1] · Selgin Al[2] · Ahmet Iyigör[3]

Received: 25 March 2022 / Accepted: 17 October 2022 / Published online: 25 October 2022

Abstract

Due to growing interest to predict and design new potential Heusler alloys by using theoretical calculations and highly functional software, research on Heusler alloys has taken great attention. From this point of view, this study considers investigation of X_2MgAl (X = Sc, Ti and Y) alloys by adopting first principles calculations for the first time. A thorough investigation has been carried out to reveal these alloys' mechanical, electronic, vibrational and thermodynamic properties. It is seen that all alloys have negative formation energies as − 0.278 eV/atom for Sc_2MgAl, − 0.058 eV/atom for Ti_2MgAl and − 0.304 eV/atom for Y_2MgAl which indicates synthesisability and thermodynamic stability. Mechanical stability investigations based on the elastic constants of alloys have revealed that all alloys are mechanically stable. The electronic band structures of alloys demonstrate that X_2MgAl (X = Sc, Ti and Y) alloys are metallic since there is no energy gap near the Fermi level. Cauchy's pressures of alloys are found as − 17.791 GPa for Sc_2MgAl, 31.404 GPa for Ti_2MgAl and − 11.759 GPa for Y_2MgAl which displays that Sc_2MgAl and Y_2MgAl are brittle and Ti_2MgAl is ductile. The phonon dispersion curves are calculated along the lines of high symmetry within the first Brillouin region. Phonon frequencies are completely positive in the full Brillouin region, which proves the dynamic stability of the $L2_1$ phases of these alloys. Several thermodynamic properties such as Debye entropy, temperature and vibrational free energy are also computed and analysed. Debye entropies of alloys follow $Ti_2MgAl > Y_2MgAl > Sc_2MgAl$ relationship.

Keywords First principle · DFT · Electronic structure · Phonon · Elastic constant

Introduction

One of the interesting classes of materials is discovered by the German Engineer Fritz Heusler, which has a composition of Cu_2MnAl [1, 2]. Whilst Cu_2MnAl is ferromagnetic, none of its elements is; this fact brought a great deal of attention to the subject. Moreover, it has been proven that ferromagnetic alloys can be designed using non-ferromagnetic elements. [3]. This group of ternary intermetallic alloys has a stoichiometric composition of X_2YZ where X and Y are transition metals and Z is either III or IV group element. Heusler alloys have shown excellent magnetic properties for wide ranges of applications such as spin-gapless semiconductors, spintronic applications, super conductivity and magnetic field–induced shape memory effect [4, 5]. Also, half-metallic property with a band gap at the Fermi level and the insulating property with opposite spin polarisations make them very worthy to reveal their structural, mechanical, electronic and dynamic properties [5–7].

Most studies so far have focused on Fe-based Heusler alloys and their electronic properties which vary from half-metallic to metallic [8, 9]. For instance, pressure-induced phase transitions and thermoelectric properties of Fe_2ZrSi were investigated by Sofi et al. [10]. The structural and mechanical properties of Fe_2TaAl and Fe_2TaGa were studied by Khandy et al. [11]. Fe_2 AlTi [12], Fe_2TiAl [13] and Fe_2CrSi [14] have been investigated in terms of their electronic and magnetic properties. Al et al. [3] studied elastic, electronic and thermodynamic properties of full Heusler X_2TiAl (X = Au, Ru and Zr) alloys.

✉ Selgin Al
selgin.al@idu.edu.tr

[1] Department of Medical Services and Techniques, Osmaniye Korkut Ata University, Osmaniye, Turkey

[2] Department of Environmental Protection Technologies, Izmir Democracy University, Izmir, Turkey

[3] Department of Machine and Metal Technologies, Ahi Evran University, Kırşehir, Turkey

The growing interest to predict and design new potential Heusler alloys by using theoretical calculations and highly functional software without the need for setting up expensive experimental set up has led us to investigate these alloys thoroughly. The density functional theory is adopted to reveal structural, mechanical, electronic, dynamic and some thermodynamic properties of Sc_2MgAl, Ti_2MgAl and Y_2MgAl full Heusler alloys. To the best of our knowledge, there is no detailed study on these alloys in the literature. This study will reveal the various properties of these alloys and will contribute to the further development of Heusler alloys. For example, elastic constants characterise material's response to the external macroscopic stress [15] which are also related to the mechanical stability, bonding characteristics, ductility and brittleness. A series of important parameters such as bulk, shear and Young's modulus, Cauchy's pressures, Poisson's ratios and lattice constants are calculated and discussed thoroughly. Electronic, dynamic and thermodynamic properties are also obtained and evaluated. Phonon properties which are critical in order to examine lattice dynamics in microscopic scale are calculated. This kind of knowledge can provide information about phase transition, thermodynamic stability, defect transport and thermal properties.

Method of calculation

X_2MgAl alloys with 4 atoms in the unit cell crystallise in the $L2_1$ crystal structure in the Fm-3 m space group as shown in Fig. 1. The computations were carried out based on the ab initio density functional theory (DFT) [16, 17] by using the Quantum Espresso software package [18]. Perdew-Burke-Ernzerhof generalised gradient approximation (PBE-GGA) was used for the exchange correlation potential [19]. The electronic wave functions were extended to a plane wave set up to a kinetic cut-off of 40 Ry and an electronic charge density of 400 Ry. For calculations in the Brillouin region, *k*-point clusters were chosen as 8×8×8. In order to select the appropriate values in cut-off energy and *k*-point selections, necessary convergences were made by obtaining the total energies corresponding to different cut-off energies and *k*-point values. To get precise results, convergence threshold was taken as 10^{-9} Ry with mixing beta of 0.7. Energy convergence of 1 mRy per atom has been satisfied for sampling of the Brillouin zone. Fermi surface integration was performed using the Methfessel-Paxton smearing technique with $\sigma=0.01$ Ry smearing parameter [20]. In order to obtain self-fit solutions of Kohn–Sham equations, lattice dynamics properties were calculated within the framework of Density Functional Perturbation Theory (DFPT) [21]. Eight dynamic matrices were calculated over a set of 4×4×4 *q*-points to obtain phonon dispersion curves and state densities along all symmetry directions. These dynamic matrices in arbitrary wave vectors were evaluated for these clusters using the inverse Fourier transform. The elastic and thermodynamics properties were calculated using thermo-pw package [22].

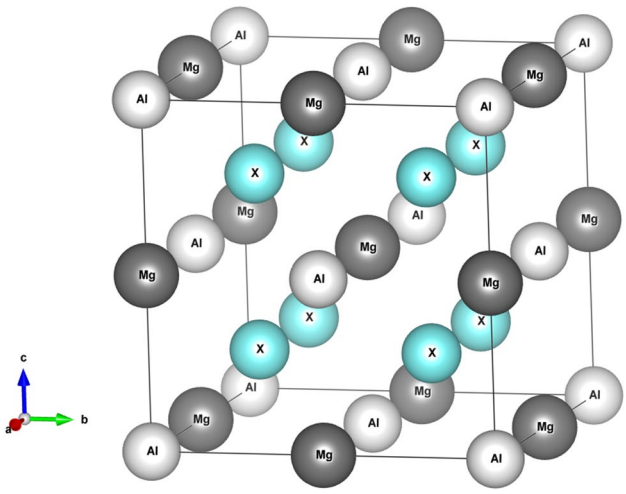

Fig. 1 Crystal structure representative of X_2MgAl (X = Sc, Ti and Y)

In order to calculate elastic constants, stress was calculated for a given strain and interval coordinates were obtained as the unit cell was fixed. There were three shear and three tensile components for stress and strain, providing six in total. Thus, a 6×6 matrix was obtained as $\sigma_i = C_{ij}E_i$ for small stress σ and strain *E*. For a cubic system, C_{11}, C_{12} and C_{44} comprise the complete set of three independent elastic constants which can be obtained by calculating the total energy as a function of the volume-conserving strains that break the cubic symmetry.

For a cubic structure, other parameters were obtained as follows:

Bulk modulus, *B*:

$$B = \frac{C_{11} + 2C_{12}}{3} \tag{1}$$

Shear modulus, *G*, was computed from the following equations where G_V is the Voigt modulus and G_R is the Reuss modulus;

$$G_V = \frac{C_{11} - C_{12} + 3C_{44}}{5} \tag{2}$$

$$G_R = \frac{5(C_{11} - C_{12})C_{44}}{3(C_{11} - C_{12}) + 4C_{44}} \tag{3}$$

$$G = \frac{G_V + G_R}{2} \tag{4}$$

Young's modulus,*E*:

$$E = \frac{9BG}{3B + G} \tag{5}$$

The Poisson's ratio, σ:

$$\sigma = \frac{1}{2}\left(1 - \frac{E}{3B}\right) \tag{6}$$

Results and discussion

Structural and mechanical properties

X_2MgAl (X = Sc, Ti and Y) is in the $L2_1$ crystal structure with the space group Fm-3 m (No. 225) which contains 2 X atoms, 1 Mg atom and 1 Al atom in the unit cell. The crystal structure representative of X_2MgAl is plotted and shown in Fig. 1. The predicted lattice constants, formation energies, bulk modulus and elastic constants are listed in Table 1. The predicted lattice constants of X_2MgAl are in good agreement with the literature [23, 24]. The formation energy is an indication of relative forces amongst atoms which can help to predict thermodynamic stability. A higher negative value of formation energy indicates better stability. It is clear from Table 1 that all alloys have negative formation energy values which implies they are thermodynamically stable.

The elastic constants can give information about physical properties and mechanical stability. For a cubic structure, there are three independent elastic constants that exist due to symmetry (C_{11}, C_{12}, C_{44}). For a stable material, these elastic constants should satisfy the Born stability criteria [25, 26];

$$(C_{11} - C_{12}) > 0, C_{11} > 0, C_{44} > 0, (C_{11} + 2C_{12}) > 0 \tag{7}$$

Equation 7 is also deducted as follows:

$$C_{12} < B < C_{11} \tag{8}$$

The predicted elastic constants of alloys satisfy the Born stability criteria and suggest mechanical stability for all three alloys based on Eqs. 7 and 8. The C_{11} value is higher than the C_{44} value for all alloys, suggesting that resistance towards the unidirectional compression is higher than that of pure shear deformation. In addition, the large bulk modulus B describes larger deformation resistance against the change in volume under external pressure. Thus, the deformation resistance of alloys can be classified as $Ti_2MgAl > Sc_2MgAl > Y_2MgAl$.

By using elastic constants, shear modulus, Young's modulus, Cauchy's pressures and Poisson's ratios of alloys are computed and presented in Table 2. The evaluation of brittleness and ductility of materials can be performed based on the B/G ratios. In the case of the higher B/G ratio than 1.75, the alloy is classified as ductile. If B/G ratio is lower than 1.75, the alloys is classified as brittle [27]. According to data given in Table 2, Ti_2MgAl is ductile whereas Sc_2MgAl and Y_2MgAl alloys are brittle materials. This is consistent with the previously reported result for Sc_2MgAl; unfortunately, no

Table 1 The calculated lattice constants (a, Å), formation energies (ΔH_f, eV/atom), bulk modulus (B, GPa) and elastic constants (C_{11}, C_{12}, C_{44}, GPa) of X_2MgAl (X = Sc, Ti and Y)

Alloys	*References*	a_0	ΔH_f	B	C_{11}	C_{12}	C_{44}
Sc_2MgAl	This work	6.923	−0.287	63.395	80.307	54.939	72.73
	Saal et al. [24]	6.913	−0.288				
	Jong et al. [23]	6.922	−0.284	65	89	53	73
Ti_2MgAl	This work	6.490	−0.058	125.431	135.850	120.222	88.818
	Saal et al. [24]	6.499	−0.087				
Y_2MgAl	This work	7.354	−0.304	57.768	74.415	46.009	57.768
	Saat et al. [24]	7.359	−0.303				
	Jong et al. [23]	7.368	−0.299	55	79	43	59

Table 2 The calculated bulk modulus (B, GPa), shear modulus (G, GPa), B/G ratios, Cauchy's pressures (C_P), Poisson's ratios (σ), Young's modulus (E, GPa), anisotropy factor (A), Vickers hardness (GPa) and Debye temperatures (Θ, K) of X_2MgAl (X = Sc, Ti and Y)

Alloys o	*References*	B	G	B/G	Cp (C_{12}–C_{44})	σ	E	A	H_v	Θ
Sc_2MgAl	This work	63.395	36.923	1.716	−17.791	0.239	91.470	5.73	5.774	408.779
	Saal et al. [24]									
	Jong et al. [23]	65	42	1.547		0.23	103.670			
Ti_2MgAl	This work	88.818	36.837	3.405	31.404	0.335	98.343	11.366	0.933	378.503
Y_2MgAl	This work	57.478	33.141	1.673	−11.759	0.243	82.271	4.067	5.484	320.426
	Saal et al. [24]									
	Jong et al. [23]	55	36	1.522		0.23	88.656			

data is found for Ti_2MgAl and Y_2MgAl in literature. Subsequently, Cauchy's pressures of alloys are estimated. A negative Cauchy pressure implies brittleness. As can be noticed from Table 2, Y_2MgAl and Sc_2MgAl alloys have negative Cauchy pressures, suggesting that both alloys are brittle. The Cauchy pressure of Ti_2MgAl is positive, which is an indication of ductility which also confirms analysis of B/G ratios.

Poisson's ratios of alloys are used to predict bonding properties and stability against shear stress. It is known that if Poisson's ratio is around 0.25, the material illustrates ionic behaviour. If it is around 0.33, the material shows metallic behaviour [28]. Based on that, it is found that Sc_2MgAl and Y_2MgAl show ionic behaviour whilst Ti_2MgAl demonstrates metallic behaviour.

Hardness (H_v) is one of the important parameters which defines the ability of a material to resist localised deformation [29]. Also, defects, grain sizes and boundaries have an impact on hardness. The calculated Vickers hardness are 5.774 GPa, 0.933 GPa and 5.484 GPa for Sc_2MgAl, Ti_2MgAl and Y_2MgAl, respectively. Sc_2MgAl and Y_2MgAl seem to display similar resistance, whereas Ti_2MgAl shows less resistance to localised deformation compared to them. Another thermodynamic property, Debye temperature (Θ), is also calculated. The Debye temperatures are $Sc_2MgAl > Ti_2MgAl > Y_2MgAl$, suggesting that Sc_2MgAl has better thermodynamic properties than the other two alloys. Moreover, the Young modulus of alloys is obtained and it is seen that Ti_2MgAl is the stiffest alloy amongst them due to having higher value of the Young modulus.

The anisotropy factor is defined as $= 2C_{44}/(C_{11} - C_{12})$ for cubic materials. This value is important in terms of determining micro-cracks, precipitation, anisotropic plastic deformation and so on [30, 31]. If this value is $A = 1$, a complete isotropy is seen; any deviation from this value indicates anisotropy. From Table 2, it is seen that all alloys display anisotropy. Hence, 2D directional changes for Poisson's ratio and the shear and Young modulus are obtained. The results are presented in Figs. 2, 3 and 4. As these figures

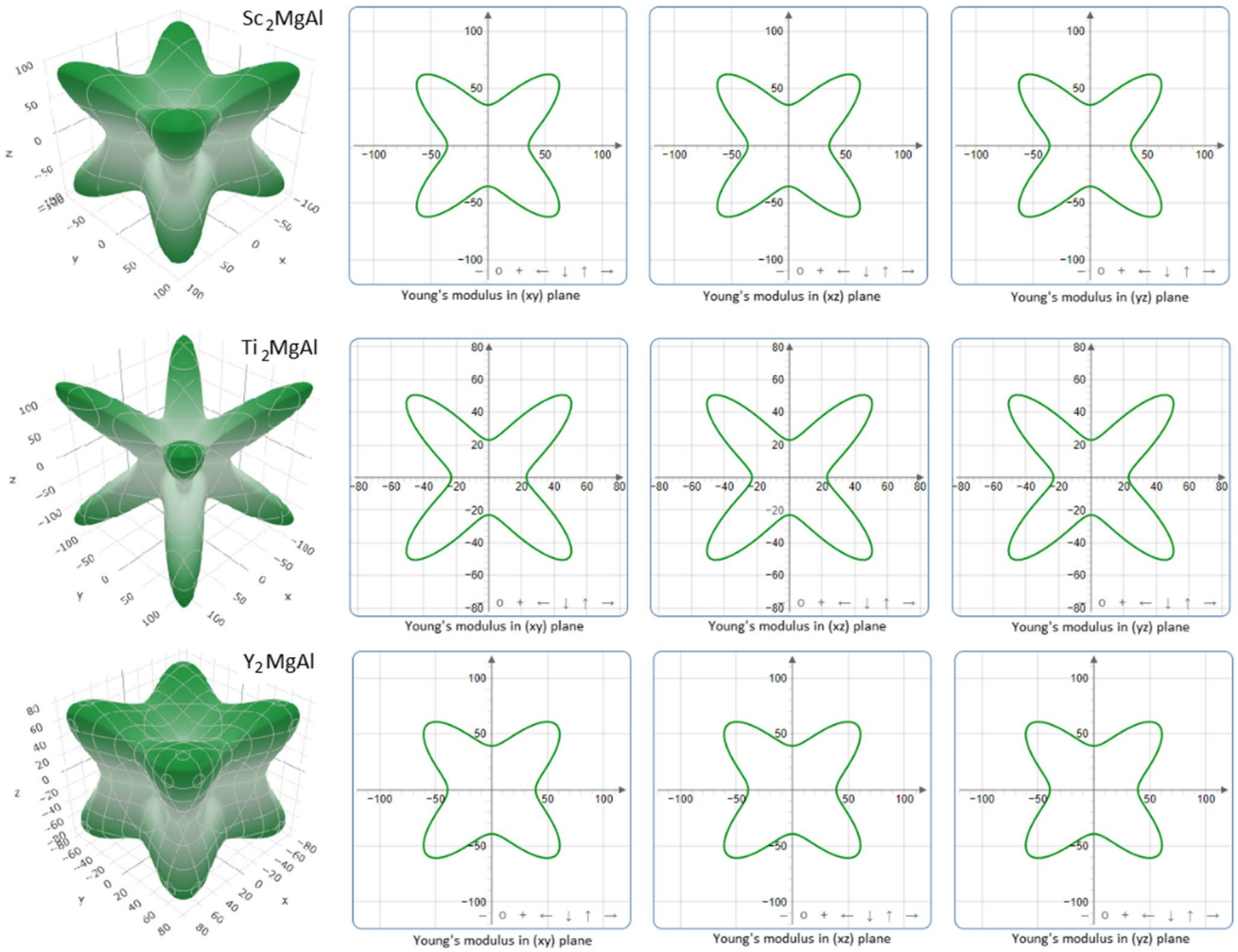

Fig. 2 2D curves of the Young modulus of X_2MgAl (X = Sc, Ti and Y)

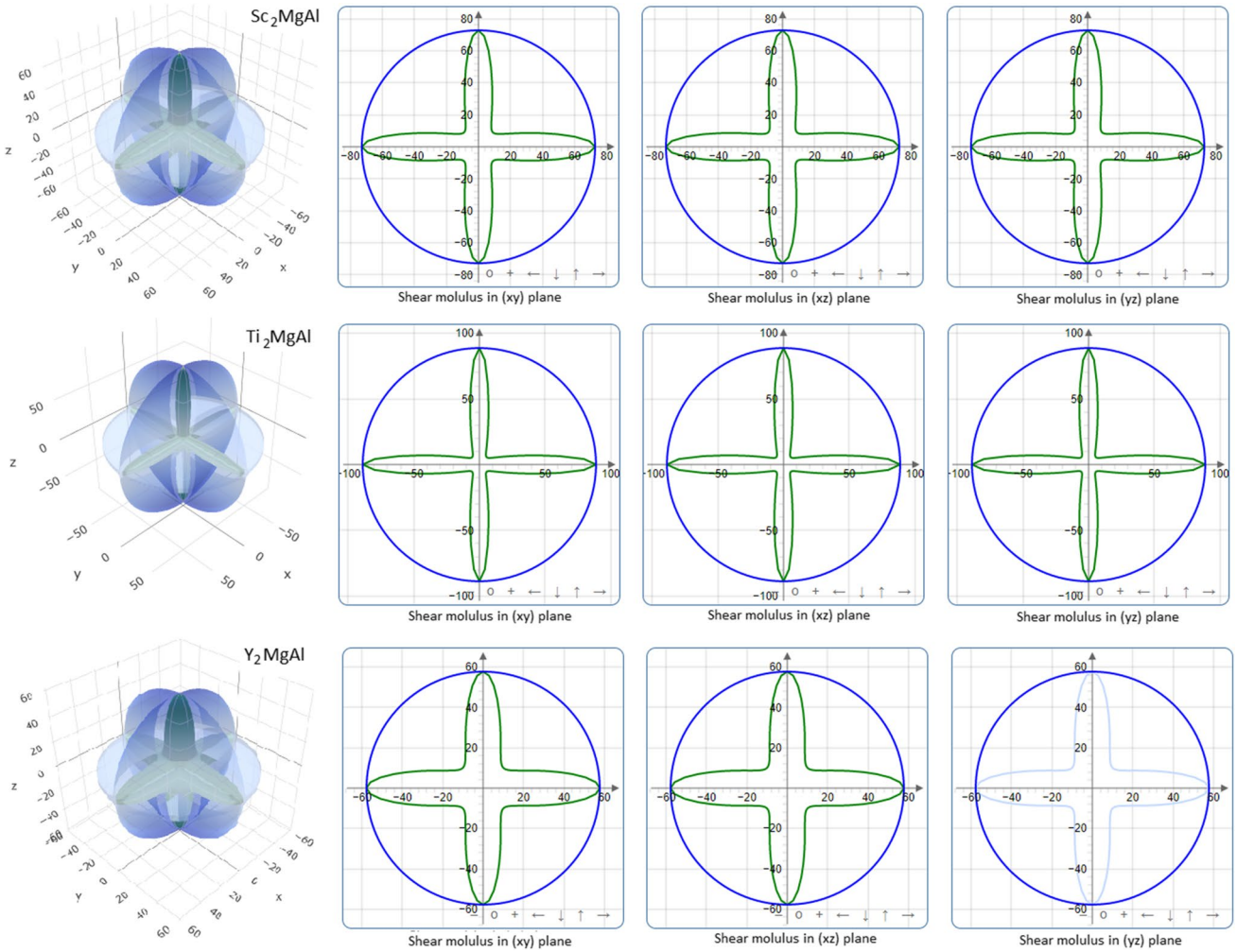

Fig. 3 2D curves of the shear modulus of X_2MgAl (X = Sc, Ti and Y)

illustrate, Poisson's ratio and the shear and Young modulus are anisotropic at all directions for all alloys.

Electronic properties

The electronic band structures of X_2MgAl (X = Sc, Ti and Y) alloys in the $L2_1$ crystal structure with the space group Fm-3 m along the high symmetry directions Γ, K, X, L and W in the Brillouin zone are computed and presented in Fig. 5 using GGA. Fermi surface is a critical parameter which allows to predict electronic structures of materials and presents surface constant energy in *k*-space [32]. Fermi level is shown as dashed lines and set to zero energy in this study. The calculated electronic band structures of alloys are similar to each other. It is seen that X_2MgAl (X = Sc, Ti and Y) alloys show metallic behaviour since there is no energy gap near the Fermi level.

To better understand the elemental contribution of alloys, the total (TDOS) and partial (PDOS) state density for alloys are obtained and presented in Fig. 6. For all three alloys, the sharp peak above the Fermi level is due to the Sc 3d state for Sc_2MgAl, the Ti 3d state for Ti_2MgAl and the Y 4d state for Y_2MgAl. As Fig. 6 shows, the main contribution to the Fermi level for the three alloys comes from the states Sc 3d, Ti 3d and Y 4d. The hybridization between the d states of Sc (Ti and Y) and Mg can be seen above the E_F from Fig. 6. The d states of Sc (Ti and Y) and Mg atoms can be discerned around − 4.0 eV for all alloys. Generally, the stability of an alloy is associated with low density states (DOS) in the Fermi energy E_F. Hence, the density of $N_{(EF)}$ states is calculated at the Fermi level.

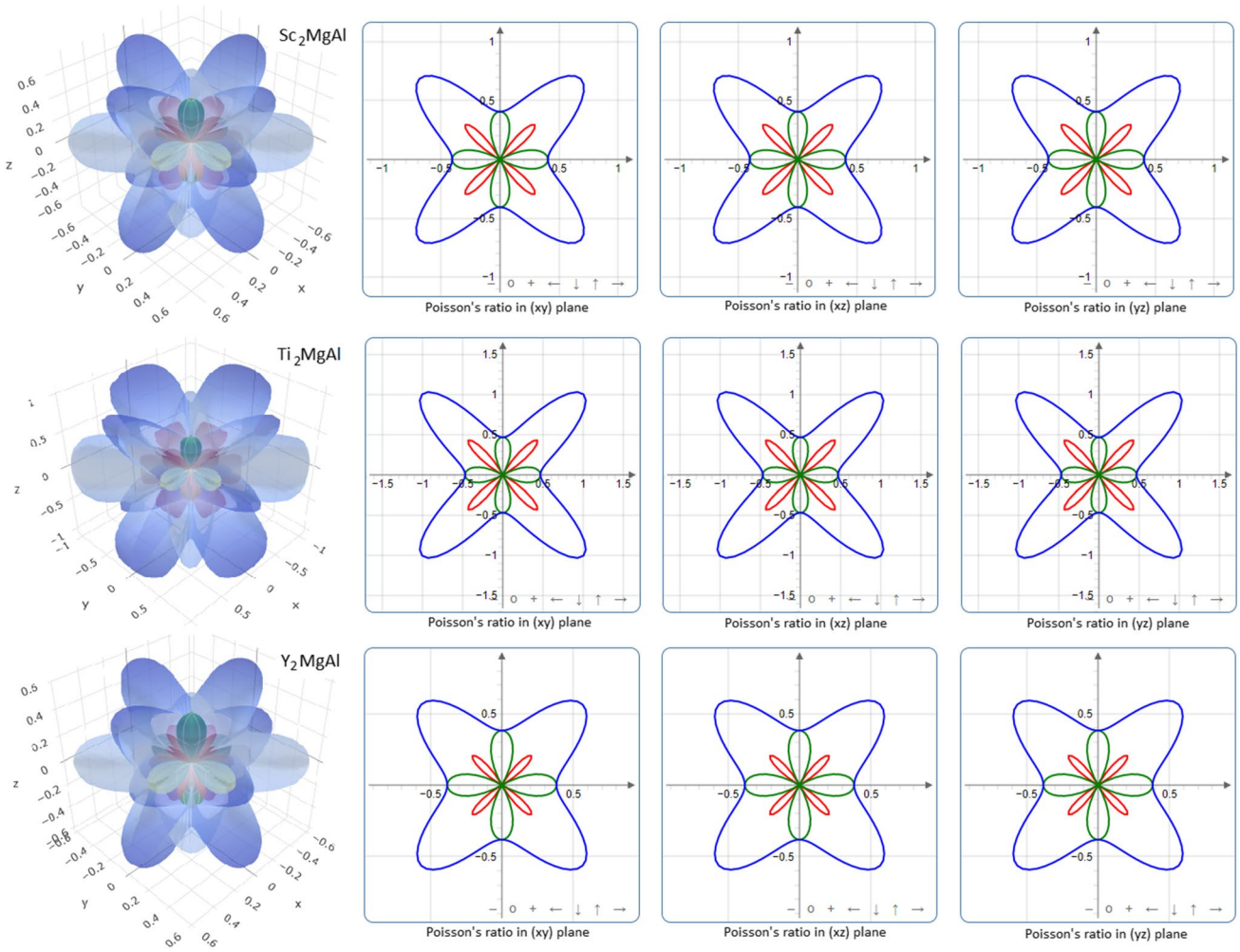

Fig. 4 2D curves of Poisson's ratios of X_2MgAl (X = Sc, Ti and Y)

Fermi level $N_{(EF)}$ state density for X_2MgAl (X = Sc, Ti and Y) is 3.06 states/eV, 4.71 states/eV and 2.75 states/eV, respectively. It can be said that Y_2MgAl has the lowest $N_{(EF)}$ value, confirming that Y_2MgAl is the more stable alloy amongst the alloys. There are no experimental or theoretical results that exist in literature to compare the electronic properties of X_2MgAl alloys in the $L2_1$ Heusler phase. Thus, the electronic properties of these alloys are presented for the first time in this study to the best of our knowledge.

Thermodynamic properties

Figure 7 demonstrates thermodynamic properties of X_2MgAl (X = Sc, Ti and Y) within the temperature range of 0 to 800 K. Vibrational and vibrational free energy are significant properties which provide information about oscillations around equilibrium in the system. Vibrational energy defines the amount of energy available internally for external interactions [33], whereas vibrational free energy defines the heat energy that can be absorbed from an outside source. As can be seen from Fig. 7, vibrational energy increases with temperature and vibrational free energy decreases after 100 K for all alloys. At low temperatures, vibrational energy is low due to the fact that atoms vibrate less because of low thermal energy. As temperature increases, thermal energy increases, and so as vibrational energy. At zero temperature, vibrational energy and vibrational free energy are expected to become equal, but not zero due to zero-point vibrations.

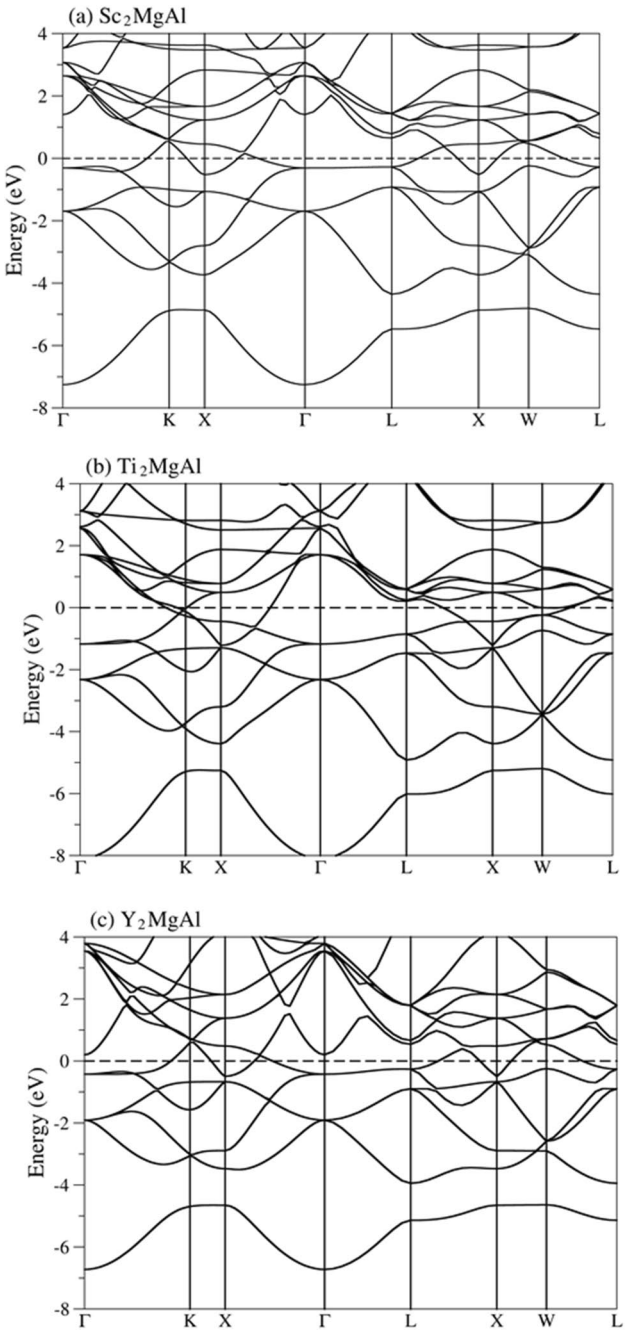

Fig. 5 Electronic band structures of X_2MgAl (X = Sc, Ti and Y)

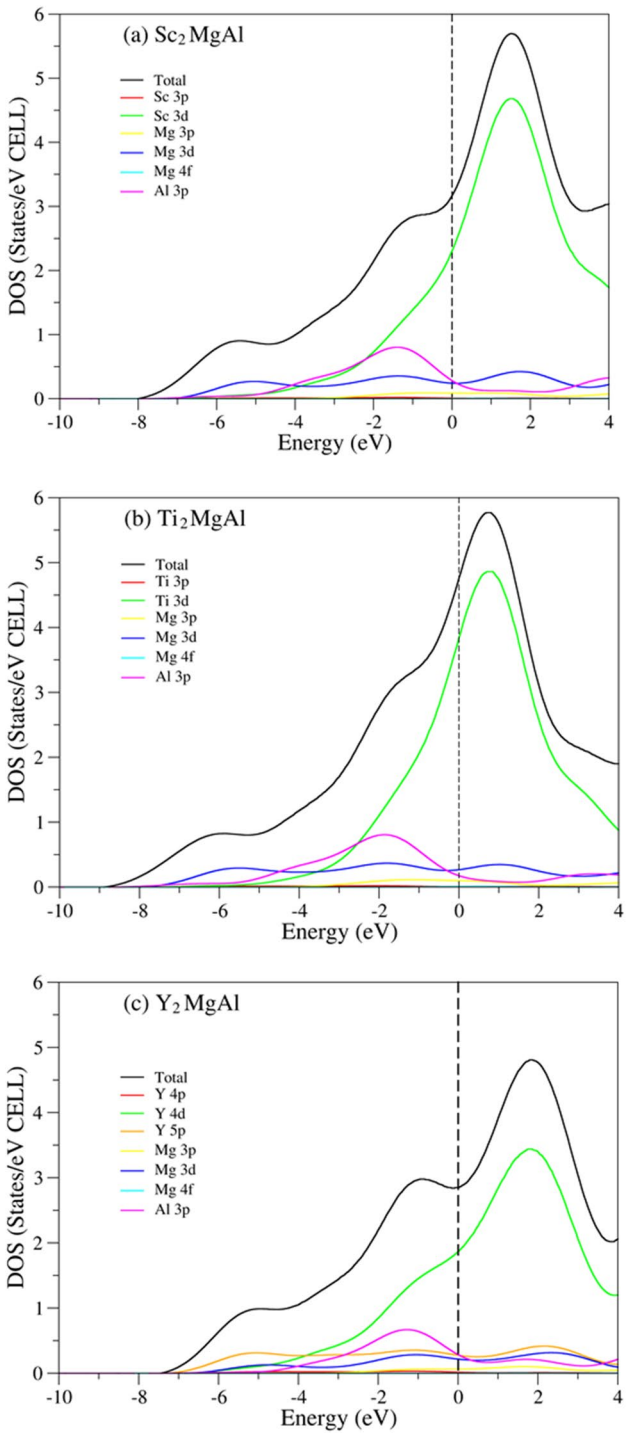

Fig. 6 Total and partial density of states of X_2MgAl (X = Sc, Ti and Y)

The temperature dependence of heat capacity at constant volume with temperature for alloys is also computed. It is clear that the heat capacity approaches the Dulong-Petit limit [34] at high temperatures. The heat capacity is lowest for Sc_2MgAl and highest for Ti_2MgAl amongst the three alloys. The Debye entropies of alloys increase as temperature increases. The entropy of a material is an indication of disorder at the atomic level and a significant thermodynamic property. The entropies of alloys follow $Ti_2MgAl > Y_2MgAl > Sc_2MgAl$ relationship.

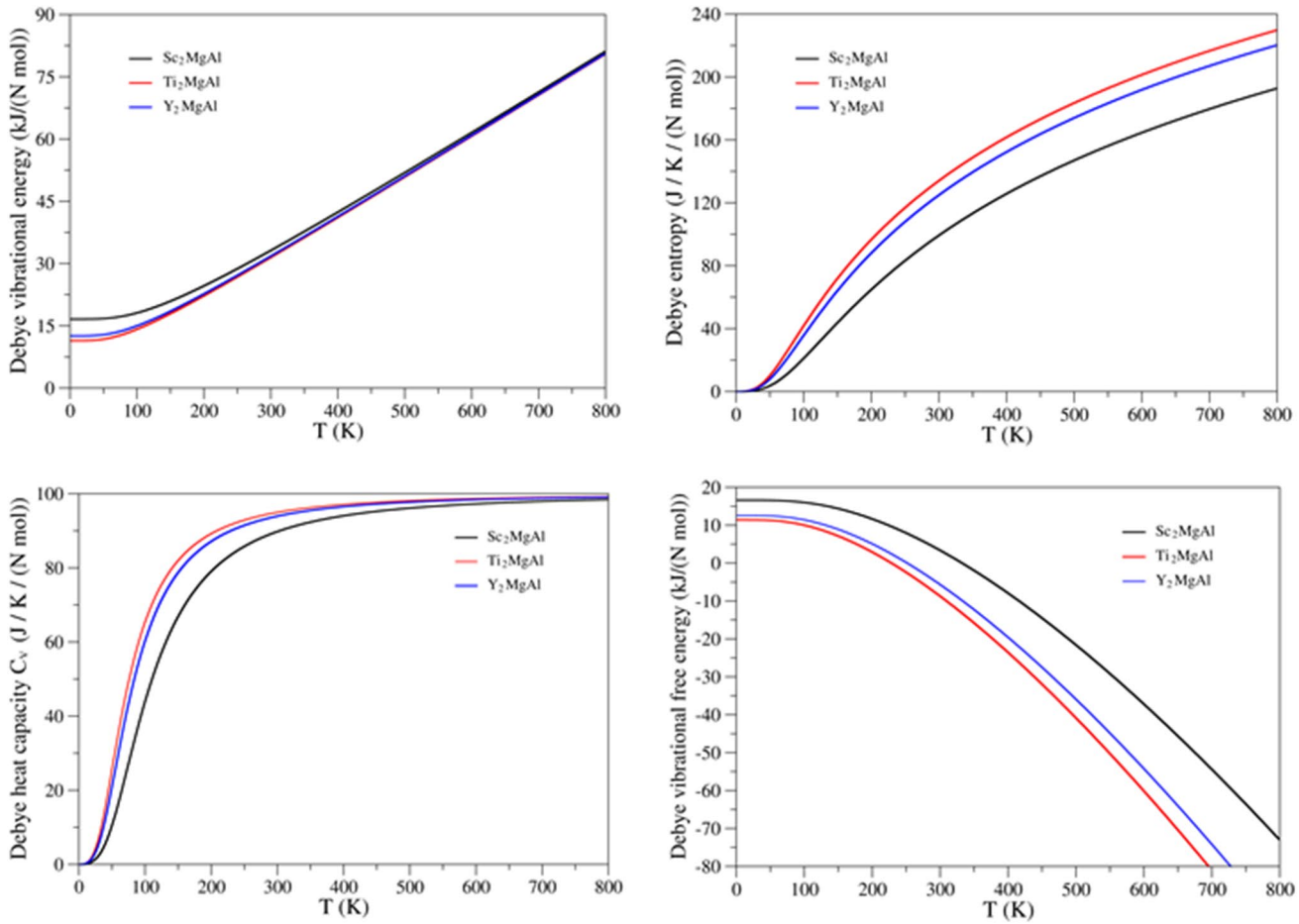

Fig. 7 Debye vibration energy, entropy, heat capacity and free energy of X_2MgAl (X = Sc, Ti and Y)

Vibrational properties

The phonon dispersion curves are calculated along the lines of high symmetry within the first Brillouin region (BZ) and illustrated in Fig. 8, and the phonon density of state of the corresponding states is shown in Fig. 9. The unit cell of X_2MgAl has four atoms in its unit cell, and therefore, at any chosen *q*-point, there are 12 vibrational modes, three of which are acoustic branches (two transverse—TA1 and TA2, and one longitudinal—LA) and nine other optical branches. Low frequency branches are generally known as acoustic branches. Two acoustic branches, one longitudinal acoustic (LA) and the other transverse acoustic (TA), are observed in regions outside the Γ-X high symmetry points. In fact, two acoustic branches are observed since some phonon branches are reduced because of high symmetry. Similarly, the high frequency region consists of optical phonon branches, many of which are transverse optical phonon modes (ωTO). As can be seen in Fig. 8, there is a phonon band gap between the acoustic and optical phonon branches due to the mass differences between Mg and Al atoms and X (X = Sc, Ti and Y) atoms. These phonon band gap values are calculated as 0.23 THz for Sc_2MgAl, 1.61 THz for Ti_2MgAl and 1.13 THz for Y_2MgAl. In order to examine these band gaps in more detail, we examine the phonon state density in Fig. 9. The phonon density of state shows two optical phonon branches separated from the optical phonon branches of lower frequencies (acoustic modes). The phonon density of state curves (PDOS) depicts that X (X = Sc, T and Y) atoms of X_2MgAl vibrate in the acoustic region (0–6.2, 0–6.15 and 0–4.6 THz regions for Sc_2MgAl, Ti_2MgAl and Y_2MgAl, respectively), and Mg and Al atoms vibrate only in the optical region (above 5.8 THz). Due to the light mass of Mg and Al atoms, they vibrate at the high frequency region and very close to each other. X (= Sc, Ti and Y) atoms vibrate at low frequency region as they are heavy

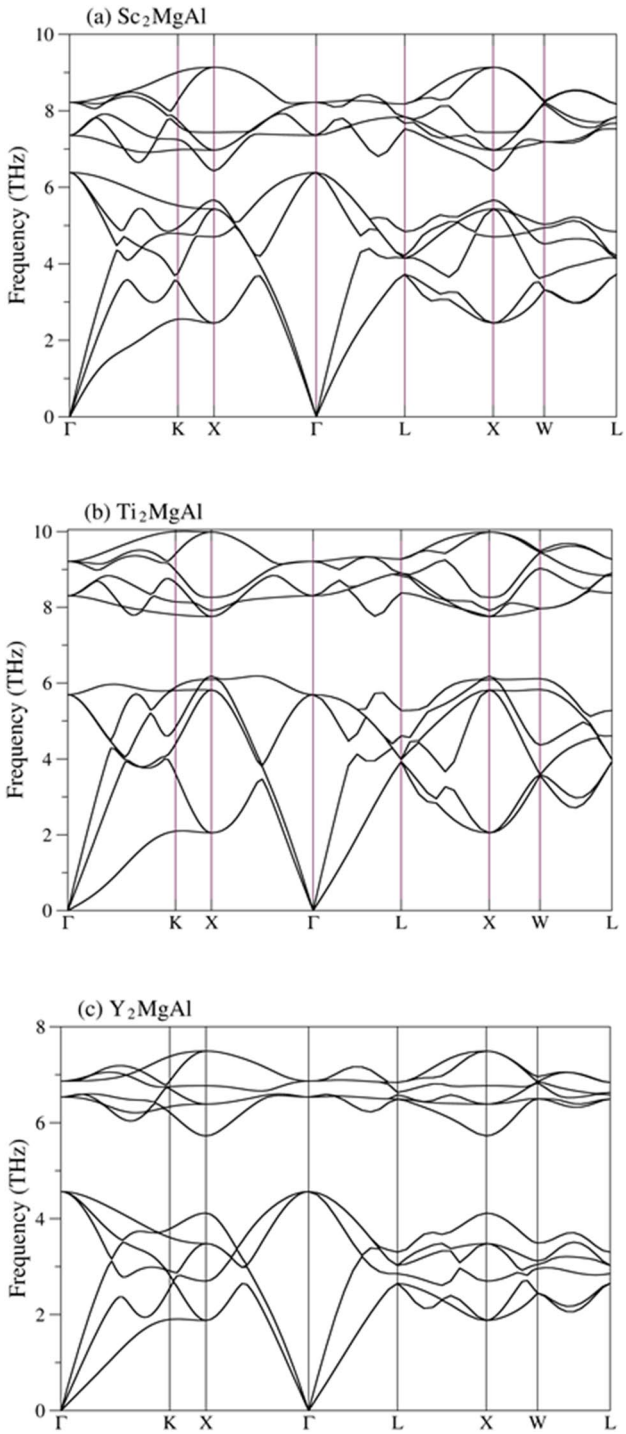

Fig. 8 Phonon dispersion curves of X_2MgAl (X = Sc, Ti and Y)

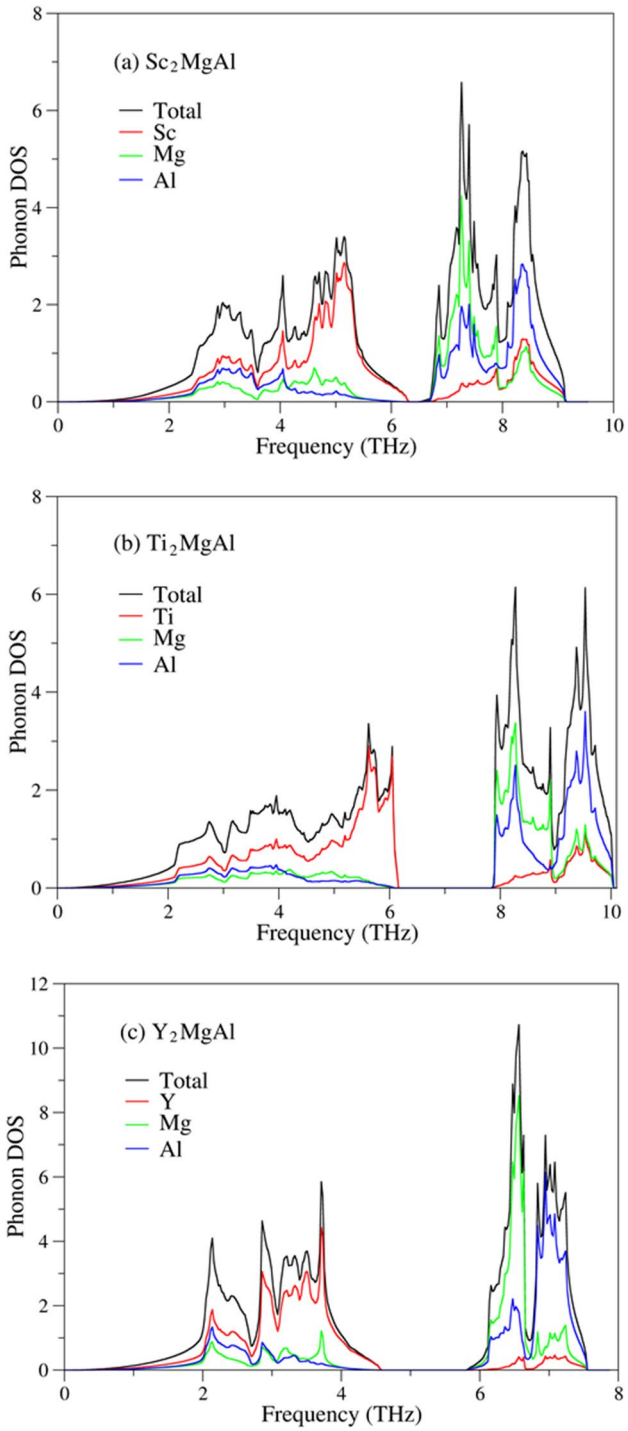

Fig. 9 Phonon density of states of X_2MgAl (X = Sc, Ti and Y)

atoms in the alloy. Zone centre phonon modes for all three alloys were determined as 6.41, 7.32 and 8.22 THz for Sc_2MgAl, 5.75, 8.32 and 9.21 THz for Ti_2MgAl and 4.61, 6.62 and 6.84 THz for Y_2MgAl.

Another important point we observed is that both Fig. 8 and Fig. 9 show positive phonon frequencies in the full Brillouin region, which proves the dynamic stability of the $L2_1$ phase of these alloys. Moreover, X_2MgAl alloys demonstrate phonon band gaps. Phonon

band gaps are desirable for various applications such as sound filters and mirrors since the gap does not allow sound to spread and only a reflection at the surface can be seen [35, 36]. This gap makes these kinds of materials suitable for insulators and mirrors. Unfortunately, there is no experimental or theoretical data available in the literature that we can compare with the full Heusler X_2MgAl alloys.

Conclusion

Several properties of X_2MgAl (X = Sc, Ti and Y) alloys are investigated for the first time in this study by means of density functional theory. Firstly, formation energies of alloys have been computed and it has been found that all alloys have negative values of formation energy. This indicates that it is possible to synthesise these alloys and they have thermodynamic stability. The mechanical stability evaluation is carried out by using elastic constants and Born stability criteria. These Heusler alloys are found to be mechanically stable which make them interesting for various applications. According to B/G ratios and Cauchy's pressures of alloys, Ti_2MgAl is ductile, whereas Sc_2MgAl and Y_2MgAl alloys are brittle. The anisotropy analysis shows that Poisson's ratio and shear and Young's modulus are anisotropic at all directions for all alloys. Electronic band structures suggest that these alloys are metallic since there is no band gap between valence and conduction band. Phonon and thermodynamic properties indicate thermodynamic stability. Phonon modes of alloys are at the positive region. Unfortunately, there is no available data for comparison of alloys. Thus, this study will serve as a reference data for future studies.

Author contribution All authors contributed equally to the preparation of the manuscript.

Data availability The data is available from the corresponding author on reasonable request.

Declarations

Competing interests The authors declare no competing interests.

References

1. Dahmane F et al (2016) Structural, electronic and magnetic properties of Fe_2-based full Heusler alloys: a first principle study. J Magn Magn Mater 407:167–174
2. Yin M, Nash P (2015) Standard enthalpies of formation of selected Ru_2YZ Heusler compounds. J Alloy Compd 634:70–74
3. Al S, Arikan N, Iyigör A (2018) Investigations of structural, elastic, electronic and thermodynamic properties of X_2TiAl Alloys: a computational study. Zeitschrift für Naturforschung A 73(9):859–867
4. Wang X et al (2017) $L2_1$ and XA ordering competition in titanium-based full-Heusler alloys. J Journal of Materials Chemistry C 5(44):11559–11564
5. Semari F et al (2018) First-principle calculations of structural, electronic and magnetic investigations of $Mn_2RuGe_{1-x}Sn_x$ quaternary Heusler alloys. Chin J Phys 56(2):567–573
6. Boumia L et al (2019) Structural, electronic and magnetic properties of new full Heusler alloys Rh_2CrZ (Z = Al, Ga, In): First-principles calculations. Chin J Phys 59:281–290
7. Hao L et al (2019) Ab initio study of the structural, electronic, magnetic, mechanical and thermodynamic properties of full-Heusler Mn_2CoGa. J Electron Mater 48(10):6222–6230
8. Sofi SA, Gupta DC (2020) Investigation of high pressure and temperature study of thermo-physical properties in semiconducting Fe_2ZrSi Heusler. Physica B 577:411792
9. Suzuki RO, Kyono T (2004) Thermoelectric properties of Fe_2TiAl Heusler alloys. J Alloy Compd 377(1):38–42
10. Sofi SA et al (2020) Investigation of pressure induced phase transition and thermoelectrics of semiconducting Fe_2ZrSi. In AIP Conference Proceedings, AIP Publishing LLC 2265(1):030346
11. Khandy SA et al (2019) Lattice dynamics, mechanical stability and electronic structure of Fe-based Heusler semiconductors. J Scientific reports 9(1):1–8
12. Friák M et al (2018) Origin of the low magnetic moment in Fe_2AlTi: An Ab initio study. J Materials 11(9):1732
13. Kurosaki Y et al (2020) Crystal growth and flat-band effects on thermoelectric properties of Fe_2TiAl-based full-Heusler thin films. J AIP Advances 10(11):115313
14. Djaidi F, Mechri H, Azzaz M (2020) Crystal structure, microstructure, and magnetic properties of the Fe_2CrSi nanostructured Heusler alloy elaborated by the mechanical alloying method. J International Journal of Materials Research 111(8):681–687
15. Akgenc, B., et al., *First-principles calculations on stability and mechanical properties of various ABO_3 and their alloys.* Materials Chemistry and Physics, 2018. **205**(Supplement C): p. 315–324.
16. Hohenberg P, Kohn W (1964) Inhomogeneous electron gas. Phys Rev 136(3B):B864–B871
17. Kohn W, Sham LJ (1965) Self-consistent equations including exchange and correlation effects. Phys Rev 140(4A):A1133–A1138
18. Paolo G et al (2009) Quantum Espresso: a modular and open-source software project for quantum simulations of materials. J Phys: Condens Matter 21(39):395502
19. Perdew JP, Burke K, Ernzerhof M (1996) Generalized gradient approximation made simple. Phys Rev Lett 77(18):3865–3868
20. Methfessel M, Paxton A (1989) High-precision sampling for Brillouin-zone integration in metals. J Physical Review B 40(6):3616
21. Baroni S et al (2001) Phonons and related crystal properties from density-functional perturbation theory. J Reviews of modern Physics 73(2):515
22. Dal Corso A (2016) Elastic constants of beryllium: a first-principles investigation. J Journal of Physics: Condensed Matter 28(7):075401
23. De Jong M et al (2015) Charting the complete elastic properties of inorganic crystalline compounds. J Scientific data 2(1):1–13
24. Saal JE et al (2013) Materials design and discovery with high-throughput density functional theory: the open quantum materials database (OQMD). J Jom 65(11):1501–1509
25. Reshak AH et al (2011) First-principles calculations of structural, elastic, electronic, and optical properties of perovskite-type

$KMgH_3$ crystals: novel hydrogen storage material. J Phys Chem B 115(12):2836–2841
26. Al S (2021) Elastic and thermodynamic properties of cubic perovskite type $NdXO_3$ (X=Ga, In). The European Physical Journal B 94(5):108
27. Yıldız GD et al (2018) Computational investigations of mechanic, electronic and lattice dynamic properties of yttrium based compounds. Int J Mod Phys B 32(20):1850214
28. Al, S., *Investigations of physical properties of $XTiH_3$ and implications for solid state hydrogen storage*, in *Zeitschrift für Naturforschung A*. 2019. p. 1023.
29. Tian J et al (2018) The effect of alloying elements on the structural stability, mechanical properties, and Debye temperature of Al_3Li: a first-principles study. J Materials 11(8):1471
30. Chang J et al (2012) Structure and mechanical properties of tantalum mononitride under high pressure: a first-principles study. J Appl Phys 112(8):083519
31. Ledbetter H, Migliori A (2006) A general elastic-anisotropy measure. J Appl Phys 100(6):063516
32. Viswanathan E et al (2019) Fermi surface and hardness enhancement study on ternary scandium and vanadium based borides by first principles investigation. J Computational Materials Science 157:107–120
33. Sunmonu RS et al (2019) Effects of Y atom substitution on the structural, magnetic, electronic, elastic, mechanical, thermodynamic and thermoelectric properties of Co_2YAl (Y = Cr, Mn) full Heusler alloys from first principles investigations. Computational Condensed Matter 21:e00412
34. Dabhi SD, Jha PK (2016) First-principles study for thermodynamic properties of wurtzite indium pnictides. Journal of Thermal Analysis Calorimetry 124(3):1341–1347
35. Arıkan N et al (2016) A first-principle study of Os-based compounds: electronic structure and vibrational properties. J Journal of Physics Chemistry of Solids 96:121–127
36. Arikan N et al (2020) Investigation of the mechanical, electronic and phonon properties of X_2ScAl (X= Ir, Os, and Pt) Heusler compounds. J Journal of the Korean Physical Society 76:916–922